Universiteit Utrecht

# Identifying the river sources and the ocean dynamics of floating plastic in the Galápagos Archipelago

Master Thesis

*Jiongqiu Ren*

*Supervisors*:

Prof. Dr. Erik van Sebille
IMAU

Dr. Stefanie Ypma
IMAU

**Institute for Marine and Atmospheric research Utrecht**

05-08-2021

**Abstract**

The increase of ocean plastic in the Galápagos Archipelago receives more and more attention in recent years. However, the sources and the potential processes that cause the locally found plastic remain unknown. In previous research, the emerged plastic on Galápagos coastlines is proved to be more likely from external sources. Among all the land-based plastic sources, riverine plastic inputs to the ocean are considered the main sources. In this research, we attribute the Galápagos plastic to the major riverine sources on the west coastlines of America based on a Bayesian inference framework. Rivers in Panama Bight and Surrounding Regions are the most likely sources. We also found that most of the particles from the Panama Bight and Surrounding Regions only arrive in the Galápagos from January to April. Particles from North Humboldt Current System also show an episodic nature of arrivals, but the arrival time is more spread throughout the years. Using a high-resolution ocean surface currents model, we simulate the pathways of virtual floating plastic particles from the river sources to the Galápagos region. We analyzed the pathways and potential ocean dynamics that cause the episodic arrivals. A Panama Jet Current is first defined in this research and is considered to be responsible for most of the plastic arriving in the Galápagos from the Panama Bight and Surrounding Regions. Humboldt Current is expected to transport most of the particles from North Humboldt Current System sources to the Galápagos. Attributing the riverine sources and identifying the ocean transporting dynamics help to better understand the episodic nature of arriving particles in the Galápagos Archipelago. Eventually, we are one step closer to predicting the arrival time of plastic in the Galápagos Archipelago.

# Contents

# 1 Introduction

## 1.1 Background

From 1950, when the plastic started to be massively produced and used, approximately 6300 million metric tons (Mt) of plastic waste had been generated until 2015 and 79% was accumulated in landfills or the natural environment (Geyer et al., 2017). A significant flux of plastic from land enters the ocean every year. Research by Jambeck et al. (2015) showed that 4.8 to 12.7 Mt of plastic entered the ocean from 192 coastal countries in 2010. With decades of plastic emission, the pollution can be found everywhere in the ocean (Barnes et al., 2010; Cozar et al., 2017; Lavers and Bond, 2017; Waller et al., 2017; Woodall et al., 2014).

Plastic is hazardous to marine life and the ecosystem in many ways. Entanglement in plastic debris, especially in discarded fishing gear, is a very serious threat to marine animals and seabirds (Derraik, 2002). Ingestion of plastic is reported to have lethal effects on a wide range of marine species (Derraik, 2002). When large plastic breaks down to microplastic, it continuously takes its toll on marine life. The most commonly used chemical components in the plastic production industry are ranked as most hazardous (Lithner et al., 2011). Lethal chemicals, such as polychlorinated biphenyls (PCBs) cause detrimental effects even at very low levels and are reported prevalent in marine food webs (Derraik, 2002).

The Galápagos Archipelago and the Galápagos Marine Reserve are recognized as UNESCO World Heritage Sites and are especially known for their unique ecosystem and biodiversity. However, even such remote and pristine islands are now found to be polluted by floating plastic (Jones et al., 2021; Mestanza et al., 2019). Microplastic was present in all seven marine invertebrate species examined, found in 52% of individuals (n = 123) confirming uptake of microplastic at the Galápagos marine food web (Jones et al., 2021).

## 1.2 Attribution of Plastic Sources

Model data indicates that most of the plastic found at the Galápagos is expected to originate from external sources (van Sebille et al., 2019). From the model results, van Sebille et al. (2019) found that the plastic enters Galápagos with little attribution to known industrial fishing grounds and large attribution to the coastlines of southern Ecuador and northern Peru. However, van Sebille et al. (2019) simulated the particle pathways from homogeneous distributed coastal sources and the type and size of the land-based sources were not considered.

Faris (1994) estimates 80% of marine plastic is from land-based sources. The land-based sources include rubbish by beachgoers and natural disasters, such as tropical storms or tsunamis, sweeping terrestrial trash into the ocean (Lebreton et al., 2012; Doong et al., 2011). However, the major pathway for land-based plastic into the ocean is river runoff (Lebreton and Andrady, 2019; Schmidt et al., 2017). In comparison to the homogeneous land-based sources in the model from van Sebille et al. (2019), modeling plastic movements from the river sources can lead to different results with more practical meaning.

It is computationally expensive to consider the size of multiple river sources in modeling the particle pathways. To optimize the computational cost, here we adopt a Bayesian inference approach to attribute the sources by probability. Pierard et al. (2022) have used the same probabilistic framework to attribute the floating plastic in the South Atlantic Ocean to the riverine inputs along the coasts of South America and Africa.

## 1.3 The Episodic Nature of Plastic Appearance

Recent studies show that buoyant marine plastic is trapped in coastal waters (Buhl-Mortensen and Buhl-Mortensen, 2017; Kaandorp et al., 2022; Lebreton et al., 2019; Onink et al., 2021). Therefore, coastal cleanup can be a promising method to mitigate the negative influence of plastic. The cleanup of a large amount of plastic on the Galápagos Islands is challenging as the park authorities have only limited resources available. It is important to make the best use of the limited resources to remove the plastic from the area as efficiently as possible.

One of the challenges for efficient coastal cleanup is the unpredicted variability of arriving time for the incoming plastic. The arriving plastic does not show up in an area at the same amount every day but with an episodic arriving pattern.

Seasonal plastic arriving pattern is caused by multiple processes, including seasonal variability of the winds, river runoff, the upwelling/downwelling periods and human industrial activities (Carretero et al., 2022). One of the frequently reported reasons for the seasonal pattern is the rain/dry season in the coastal area. The highest amount of microplastic is observed in multiple places during the rainy season, when the environment is under influence of the highest river flow, such as the South China Sea (Tsang et al., 2020), the Yellow Sea (Liu et al., 2020), the coastal sea at Ria de Vigo of Spain (Carretero et al., 2022) and the Goiana Estuary on the Northeast coast of Brazil (Lima et al., 2014).

However, the seasonal pattern for coastal plastic is not always caused by river discharge. Cheung et al. (2018) reported that the highest amount of microplastic was found in dry seasons in the coastal waters of Hong Kong and there was no correlation found with the river outflow. Jiang et al. (2020) also reported the highest amount of microplastic in dry seasons in the coastal water of the South Yellow Sea. In this region, the seasonal abundance of microplastics is positively correlated with seawater salinity, which they believed to be caused by the Yellow Sea Warm Current during the same season.

The above research reported on the estuarine regions or coastal areas with direct connection to big continents. In comparison, the Galápagos Archipelago is isolated in the Eastern Tropical Pacific, with a large fraction of plastic coming from external sources. The ocean dynamics around the Galápagos are likely to be the reasons causing the episodic appearance of coastal plastic. If we can better understand the ocean dynamics causing the episodic appearance of the Galápagos plastic, we can then make more accurate predictions to help the cleanup operations within the area.

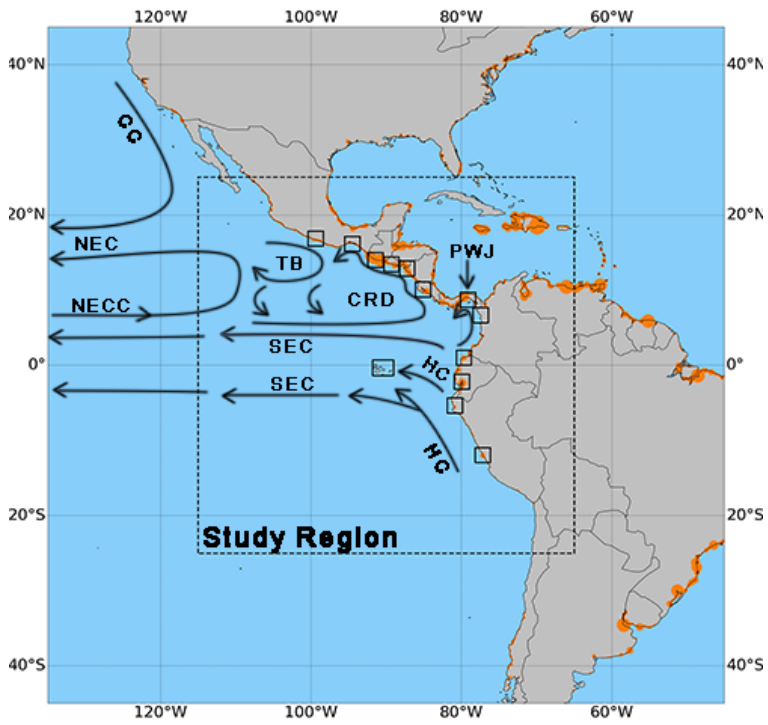


Figure 1: Map of the Eastern Tropical Pacific. The study region in this research is in the dashed-line box. The dominant ocean dynamics are North Equatorial Current (NECC), North Equatorial Countercurrent (NECC), South Equatorial Current (SEC), California Current (CC) and Humboldt Current (HC). There is a cyclonic eddy-like geostrophic circulation, termed as Costa Rica Dome (CRD) and an anti-cyclonic eddy-like geostrophic circulation, termed as Tehuantepec Bowl (TB). The Panama Wind Jet (PWJ) is also shown in the figure. The orange circles are the riverine plastic inputs from model data (Meijer et al., 2021), of which the size represents the amount of the inputs. The green boxes are the clustered river sources.

## 1.4 Ocean dynamics in the Eastern Tropical Pacific

Attributing the episodic arrival of the Galápagos plastic to the ocean dynamics in the Eastern Tropical Pacific is not easy, due to the complex and unique ocean phenomena within the area (Figure 1). The eastward North Equatorial Countercurrent (NECC) dominates the north of the region. While in the central Pacific the NECC is predominantly geostrophic, in the Eastern Tropical Pacific, the eastward flow consists mainly of the Ekman surface currents driven by the southerly wind across the equator (Kessler, 2002). The Ekman-contributed NECC is strongly seasonal modulated, weak in boreal spring and strong in boreal autumn. During August-January, the NECC extends all the way to the west coast of the Americas (Kessler, 2006). The surface South Equatorial Current (SEC) covers a big area in the Eastern Tropical Pacific. Compared to the central Pacific where the SEC is strong, the SEC east of 110° is weak (Kessler, 2006).

In the south of the study region, there is the Northern Humboldt Current System (NHCS:

$79°W - 90°W;\ 0° - 20°S$) (Grados et al., 2018). The surface circulation of the region is dominant with the Humboldt Current (HC). The HC veers progressively westward and feeds the SEC (Grados et al., 2018).

The Panama Bight and Surrounding Regions are defined in the previous research (PBSR: $0° - 9°N;\ 73°W - 90°W$) (Chaigneau et al., 2006; Rodríguez-Rubio et al., 2003). The region is dominated by the Panama Wind Jet, a seasonal wind that enters the Panama Bight via the Isthmus of Panama (Rodríguez-Rubio et al., 2003). The Panama Wind Jet is strengthened during the spring (Wooster, 1959), and drives a Panama Jet Current during January-March (Chaigneau et al., 2006). However, the Panama Jet Current and its seasonal variation did not receive enough focus from the researchers. The scientific community was more interested in the upwelling caused by the Panama Wind Jet (Chaigneau et al., 2006; Wooster, 1959) and its influence on biological productivity (Rodríguez-Rubio et al., 2003).

## 1.5 Summary

In order to improve the efficiency of ocean cleanup, it is important to understand the episodic nature of plastic arrival at the Galápagos Archipelago. The episodic arrival of plastic is dependent on the spatial distribution of sources and the ocean dynamics that transport the plastic. The combination of source distribution and Lagrangian simulations is conducted in some previous research but there has been little research connecting the temporal variability of plastic arrival to ocean dynamics.

This research will specify the riverine plastic sources on the west coast of the Americas and investigate the major surface ocean processes that transport the plastic in the Eastern Tropical Pacific. Eventually, we propose the following research questions:

1. What are the major riverine plastic sources for Galápagos plastic?
2. When does the plastic arrive at the Galápagos?
3. What are the major ocean dynamics that are responsible for the Galápagos plastic?

# 2 Methods

This chapter will introduce the methodology to attribute the Galápagos plastic to the river sources and ocean dynamics. Section 2.1 introduces the settings of the riverine plastic inputs model. Given the different resolutions between river and ocean data, the river data has to be preprocessed to be applicable for the Lagrangian simulations. The setup for the Lagrangian model is explained in section 2.2. A Bayesian framework is used in this research to make attribution to different river sources and the theory is introduced in section 2.3.

## 2.1 River Sources

It is impossible to make reliable estimates of the amount of plastic inputs to the ocean (Derraik, 2002). Only a few regional studies have reported the amount of plastic contamination in the freshwater system (Wagner et al., 2014). Furthermore, the methodology for river sources of ocean plastic is not yet standardized, making it difficult to construct a global database (Dris et al., 2015). Therefore, the river sources are often estimated based on a probability framework.

Meijer et al. (2021) propose a probabilistic approach to calculate the riverine emission by multiplying the mismanaged plastic waste ($MPW$) and the probability of which into the ocean.

$$M_E = \sum_n MPW \times P(E) \tag{1}$$

$MPW$ mass ($kg \cdot year^{-1}$) is from a recent estimate by Lebreton and Andrady (2019) on a 30 by 30 arc seconds resolution. $P(E)$ is the probability of the $MPW$ being transported into the ocean by rivers in each grid cell. The total annual emission $M_E$ of plastic into the ocean at a river mouth is then computed by accumulating this product for all n grid cells contained in the river basin (Meijer et al., 2021). The geographical location of the major rivers and river basins is based on the data set and paper from Ghiggi et al. (2019), with a 0.5° spatial resolution.

The probability $P(E)$ of the $MPW$ transported into the ocean is calculated by taking account of three major events, mobilization on land $P(M)$, transport from land to a river $P(R)$, and transport from the river to the ocean $P(O)$.

$$P(E) = P(M) \times P(R) \times P(O) \tag{2}$$

To incorporate as much physics and mechanisms into the model, Meijer et al. (2021) took into account wind forcing, precipitation, terrain slope, the roughness of the landscape, the discharge of the river, and the distance of the rivers to the ocean. The modeled emission at river mouths gives a good order-of-magnitude correlation (coefficient of determination, $r^2 = 0.74$, $n = 74$) with the observation data of the riverine plastic inputs into the ocean. However, the model does not give the seasonal variation of the river plastic inputs (Lebreton and Andrady, 2019; Meijer et al., 2021).

In this research, the study region is restricted between $25°N$-$25°S$ and $115°W$-$65°W$ (Figure 1). The reason why this range is chosen is based on the preliminary research by van Sebille et al. (2019). In the research, van Sebille et al. (2019) found only very few of the particles released south of $16°S$ or north of $3°N$ reached the Galápagos. However, from the river data used in this research, some major rivers are found north to $3°N$ and $16°S$, for accuracy consideration, $25°N$ and $25°S$ are chosen as the north and south boundary for the latitude range.

There are a few challenges to adapt the river source data to the ocean general circulation model used in this research. The ocean general circulation model has a courser resolution than the riverine inputs data set. The first challenge is to convert the riverine emission data from finer-resolution grids to courser-resolution grids in the ocean field. We selected the annual emissions and locations of the river mouths in the study region. The locations were moved to the center of the closest ocean grid cell in the courser flow field. We summed the emissions of the river mouths that shared the same ocean grid cell. This method is based on the method and algorithm by Pierard et al. (2022).

Since the river source data set is constructed for the coastal grid cells for the globe, but only the river sources on the Pacific side of the coast of the Americas are interested in this research, the second challenge is to select the Pacific-side coastal grid cells in the flow field. Pierard et al. (2022) selected the river mouths on the Atlantic side of South America between $0°$-$45°S$. Within the latitude range in that research, the distance between the Pacific and Atlantic sides is relatively big. It is applicable to use a simple polygon mask to select the data. However, in this research, the distance between both sides is small at some places. As a result, simple polygon masks are not applicable in this research. Here we propose a new algorithm to detect the Pacific side of the coast grid cells. In the first step, we find all the coastal cells in the ocean grid and select the most northern grid of the Pacific coast as the start grid. In the second step, we search for the coastal cell that is closest to the start grid as the next grid. Since all the Pacific coast grids are adjacent and the Atlantic grids are at least a few grids away from the Pacific grids, this algorithm can naturally avoid the Atlantic grid cells. We repeat the second step to find the next grid, but a judgment step is added. In the judgment step, multiple conditions are judged to select the next grid. One of the most important judgment is to detect the cell that has not been selected before. More details on the judgment step can be found online at https://github.com/OceanParcels/Galápagos_highresflow.

The third challenge is the normalization of the riverine emission. The river data set uses a mass unit, but outputs from the simulations in this research (introduced in section 2.2) use the number of particles. The riverine emission is therefore normalized to the percentage by dividing by the sum of riverine plastic inputs within the study region.

There are no big river basins but plenty of small watersheds and river mouths along the Pacific coast of the Americas. Therefore, we combine the rivers that are geographically close to each other into one river cluster, defined as a 2-by-2-degree box. Each river cluster consists of 576 grid cells. The size of each river cluster is the sum of all the normalized emissions within it. Eventually, the top 12 river clusters are selected representing 93% of the river plastic inputs within the region (Table 1). There are three clusters located in the North

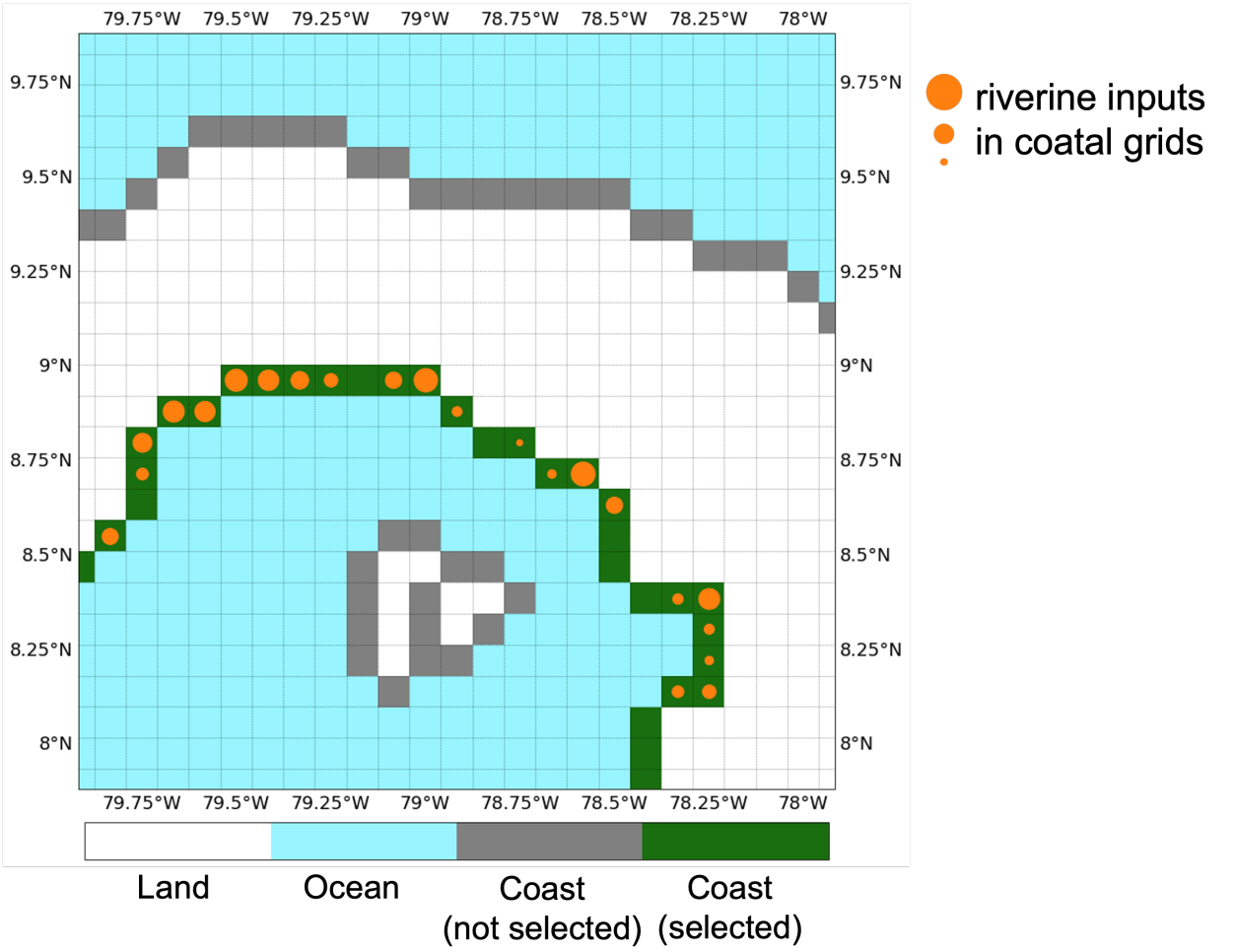


Figure 2: The 2-by-2 degree river cluster at Panama. White cells are land cells. The grey cells are coastal cells that are not selected by the algorithm, while the green cells are the selected coastal cells. The cells with orange dots are the releasing cells, with the size of the dots the river sizes.

Humboldt Current System (NHCS) (Grados et al., 2018): Guayaquil, Parachique and Lima. Three locate in the Panama Bight and Surrounding Regions (PBSR) (Chaigneau et al., 2006; Rodríguez-Rubio et al., 2003): Panama, Cacique, and Esmeraldas. The remaining 6 clusters are north to the PBSR: Acapulco, Salina Cruz, Tecojate, La Colorada, Fonseca and Chira. Figure 2 shows an example of the Panama cluster. In the later section, we also use river source as an alternative term for river cluster, since river source is more intuitive when compared with other literature.

## 2.2 Lagrangian Model Setup

To analyze the origin and arrival time of particles, we performed Lagrangian simulations where we tracked the particles from each river cluster. In the simulation, the floating plastic debris is idealized as virtual particles at the surface of the ocean velocity field, with no other

Table 1: River size

| River cluster | River size |
|---|---|
| Acapulco | 1.1% |
| Salina Cruz | 2.5% |
| Tecojate | 13.5% |
| La Colorada | 4.8% |
| Fonseca | 7.4% |
| Chira | 1.0% |
| Panama | 50.4% |
| Cacique | 9.6% |
| Esmeraldas | 0.6% |
| Guayaquil | 1.9% |
| Parachique | 0.1% |
| Lima | 0.3% |
| Total | 93.2% |

physical and geometric information. The ocean velocity field is provided by a global high-resolution monitoring and forecasting system PSY4V3R1, which is based on version 3.1 of the NEMO ocean model. For the purpose of this research, we use the surface velocity field, which has a 1/12° resolution. PSY4V3R1 provides daily ocean data, and we use the data from 2007-01-01 to 2021-12-31.

The Lagrangian simulations are done with OceanParcels Version 2.3 (Delandmeter and van Sebille, 2019), Parcels hereafter. Parcels allow spatial and temporal interpolation of the fields following the C-grid interpolation scheme (Delandmeter and van Sebille, 2019).

A total number of 14 simulations are conducted, with the starting year from 2007 to 2020. Each simulation last for 2 years. During each simulation, a total number of 100,010 particles ($274\ par/day\ \times\ 365\ days$) are released within each river cluster during the first year and tracked down until the last day of the second year. The same number of particles is released each simulation each river cluster. Within each cluster the probability of which releasing cell to release the particles is based on the riverine plastic input size of each releasing cell. 274 particles are released every day but are randomly distributed at different hours of one releasing day. The particles are only released during the first year and tracked down until the last day of the second year. The advection is calculated by fourth-order Runge-Kutta method with a timestep of 1 hour and the location of each particle is stored every day.

The mesoscale eddies can be resolved without being parameterized as an eddy diffusion due to high resolution of the velocity field from NEMO. However, diffusion is not included in calculating trajectories, which creates a problem on stochasticity. In the real ocean, because of the diffusion, even two particles are released at the same time and at the same location, the trajectories thereafter are different. But, in numerical models, if two particles are released at the exact same time and location, they will end up with two identical trajectories. As

a result, other measures need to be taken to increase the stochasticity of releasing strategy. Using river clusters instead of river mouths is one of the measures. The particles released at the same time have a probability to be distributed on different river mouths within each cluster and the probability is based on the size of the emission of the river mouths. Another measure is to randomly distribute the 274 particles at different hours during one releasing day. Sensitivity analyses are done for releasing half the number of particles in each cluster. And they show the same probability for particles to arrive at the Galápagos from each simulation, which proves the releasing strategy used in this research is enough to make valid conclusions.

The particles are released for at least 1 year to investigate the seasonal variability. However, the trajectories are not tracked for more than 2 years mainly due to the following reason. It is discovered that most particles arrive at the Galápagos within 3-4 months (van Sebille et al., 2019). Although the age of arriving particles can be as long as 5 years, the number of those particles is relatively small, and it is considered not worthy to extend the simulation time.

The Galápagos Archipelago region is defined as the same way in the previous research (van Sebille et al., 2019), a box at $91.8°W$-$89°W$ and $1.4°S$-$0.7°N$ (Figure 1). If a particle reaches the region once, it is counted as arrived at the Galápagos.

## 2.3 Bayesian Framework

The Bayesian inference framework uses Bayes' theorem to calculate the conditional probability of an event based on the prior knowledge of conditions that might be related to the event. Specifically, the research goal is to estimate the attribution which is the conditional probability ($p(S_i|G)$) of a particle found at the Galápagos region ($G$) would come from a certain source ($S_i$). The Bayes' theorem allows to calculate the conditional probability by

$$p(S_i|G) = \frac{p(G|S_i) \cdot p(S_i)}{p(G)} \tag{3}$$

where $p(S_i|G)$ is the attribution, $p(S_i)$ is the size of the source (prior knowledge), $p(G|S_i)$ is the arriving rate from a certain source and $p(G)$ is the normalizing factor. The size of the source $p(S_i)$ has been explained in section 2.1. The arriving rate $p(G|S_i)$ is obtained from the simulations by the fraction of the arrive-at-Galápagos to the total released particles at each source. The particle arriving at the Galápagos is defined in section 2.2.

In eq. 1, the normalizing factor $p(G)$ is the sum of attribution to all the possible plastic sources. In theory, if attribution to all the sources is incorporated, the normalizing factor $p(G)$ is one (Carlin, 2008; Pierard et al., 2022), but in this case, only attribution to the 12 river clusters is considered. As a result, the normalizing factor is computed as

$$p(G) = \sum_{i=1}^{12} p(G|S_i) \cdot p(S_i) \tag{4}$$

By substituting eq. 4 into eq. 3, the attribution to each river source is

$$p(S_i|G) = \frac{p(G|S_i) \cdot p(S_i)}{\sum_{i=1}^{12} p(G|S_i) \cdot p(S_i)} \tag{5}$$

which is the alternative form of Bayes' theorem.

To analyze the arriving patterns, the dates and ages of each arriving particle is recorded. The number of particles arriving at the Galápagos on each simulation day is counted and normalized by the total number of arriving particles of that simulation. At last, the arriving patterns are made for each source in each simulation.

## 2.4 Process Analysis

This section will explain the methodology to analyze the potential ocean processes that transport the particles. The size of the source will not be considered when conducting the process analysis. This is because that the difference between some of the river sizes is big, which masks out the contribution of transporting particles by some of the ocean dynamics.

### 2.4.1 Pathways

During the Lagrangian simulation, the geographic location of each particle is recorded everyday after being released from each source. The occurrence in a grid cell is calculated by counting the number of the particles in that cell over the simulations from all the years. After a particle is released, it contributes to one occurrence everyday in one of the ocean grids. Computing the occurrence of all the grids in the study region, we can form an occurrence map. The occurrence density map is further calculated from normalizing the occurrence map by the total occurrence from all the ocean grids in the study region. Fig. 3a show the integrated occurrence density map from all 12 sources. The hotspots in the density map represent for regions that particles are likely to converge, thus, in a more practical meaning as the pathways for particles to the Galápagos.

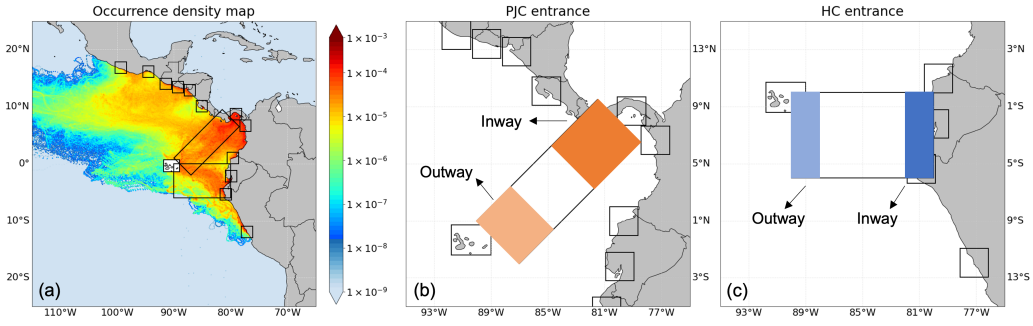


Figure 3: The integrated occurrence density map is shown in (a) with twelve river clusters in square boxes and the two entrances in rectangular boxes. (b) and (c) show the Panama Jet Current entrance and Humboldt Current entrance relatively. The inway and outway of the entrance are in dark and light colr respectively.

### 2.4.2 Entrances to the Galápagos

By the definition of the pathways, the particles from each source are most likely to take the pathways to the Galápagos and the 12 sources generate 12 pathways. However, some of the pathways converge and eventually result in two major entrances into the Galápagos region, one from northeast and another from east (figure 3a).

In this research, we assume that the currents are the dominant ocean dynamics occurring along the pathways (figure 1). The ideal intention is to resolve every ocean dynamic along every pathway, but that requires a lot of work for a master project. The more upstream the more spread the pathways are and the more currents need investigated. We only focus on the downstream of the pathways where the two entrances take place. We try to find out what the two currents are that drive the particles arrive at the Galápagos from these two entrances. The entrance from the both directions are restricted in the two boxes in the corresponding directions relatively (figure 3b and 3c).

### 2.4.3 Particle Behaviors

The occurrence density map only shows the locations where the pathways take place but not the behaviors of the particles. Although we know from the intuition that the particles move from the sources to the Galápagos, from the density map itself the particle behaviors are not evident. For example, in the northeast entrance box, the particles moving from the upper end to the lower end are shown as same as those moving from the lower end to the upper end in the occurrence density map (figure 3a). We need to constrain the entrance box with a rule of particle behavior to quantify the particles that have actually been transported via the entrance pathway.

Figure 3b and 3c show the method of constraining the particle behaviors in two entrance boxes. There are two regions within each box, inway and outway. Along a particle trajectory, when the particle is detected in the inway region it becomes a potential particle. After 40 days when it enters the inway, if it ever reaches the outway region it is considered a transported particle by the corresponding dynamic. The total number of the transported particles is calculated for quantification in section 3.2.1.

# 3 Results

The methodology in the previous chapter is introduced to achieve the research goals. Section 3.1.1 shows the overall attribution of the Galápagos plastic to the 12 river sources averaging over 14 simulations. The temporal distribution of the particles arriving at the Galápagos is studied in section 3.1.2. Episodic arriving patterns are discovered.

In section 3.2 the occurrence density map is produced to study the potential particle pathways. The pathways give information on the possible locations where the ocean dynamics are responsible for the particles transport. In section 3.2.1, two major entrances are discovered among all the pathways. The behaviors that the particles take to pass the entrances are discussed. In section 3.2.2, the ocean dynamics that drive the particle behaviors are discovered.

## 3.1 Source Attribution

### 3.1.1 Arriving Rate and Attribution

The same number of particles are released from each river source and the arriving rate is demonstrated in the left panel of figure 4. There are 6 river sources north to Panama Bight and Surrounding Regions (PBSR) (Chaigneau et al., 2006; Rodríguez-Rubio et al., 2003), Acapulco, Salina Cruz, Tecojate, La Colorada, Fonseca and Chira. Hereafter we name these 6 river sources as the Northern Region (NR) sources. For the particles from NR sources, around 1.0% of the released particles find their ways to the Galápagos. Panama and Cacique, both lying in the northeast corner of the PBSR, are more likely to send particles to the Galápagos, with a probability of 12.37% and 11.44% respectively. At the south edge of the PBSR is the Esmeraldas, where 3.68% of the released particles eventually arrive at the Galápagos. In the North Humboldt Current System (NHCS) (Grados et al., 2018), there are three river sources, Guayaquil, Parachique and Lima. The particles from Parachique are most likely to end up at the Galápagos, with a probability of 23.36%. 2.57% and 1.04% of the released particles arrive at the Galápagos from Guayaquil and Lima, respectively. Considering the large number of released particles from each source, even the lowest arriving rate, 0.68% for Fonseca, results in 9521 virtual plastic particles arriving at the Galápagos region from all the simulations.

However, the above results do not consider the actual size of the river sources. By using the Bayesian framework, attribution is calculated combining the river size and the arriving rate, shown in the right panel of figure 4. 94.33% of the Galápagos plastic originates from Panama and Cacique, specifically, 80.26% from Panama, 14.07% from Cacique. The NR sources contribute to 4.45% of the arriving particles, with Tecojate contributing 2.29% leading the rest. Although the arriving rates of the NR sources are similar, the stand-out river size (from table 1) makes the attribution to Tecojate higher than the others. Also because of the relatively small river size, the attribution to Parachique is small even when the arriving rate is the highest.

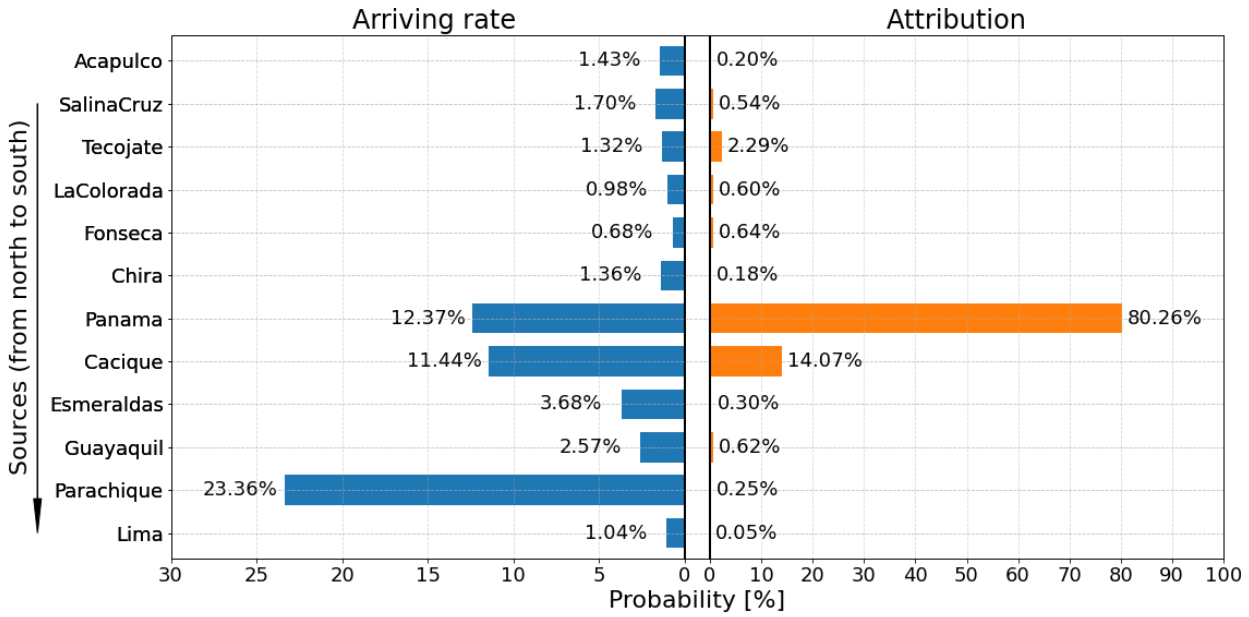


Figure 4: The probability calculated from the Bayesian framework. The left panel shows the arriving rate from each source. The right panel shows the attribution of the Galápagos particles to different river sources.

### 3.1.2 Arriving Patterns

The arriving patterns are derived as follows. For each simulation at each source, the arriving rate is calculated weekly and normalized by the total arriving rate of the simulation. The arriving patterns are averaged over 14 simulations. Eventually, 12 arriving patterns are derived for 12 sources. We group the arriving patterns that show resemblance in the pattern itself, shown in the left panel of figure 5. The patterns are divided into 3 categories which is in consistency to the geographical-based classification of river sources introduced in the texts above. The arriving patterns of all 12 sources are shown in appendices (figure 11).

There is a similarity between the NR and PBSR arriving patterns, where a chunk of particles arrive at the Galápagos in the boreal spring of the second year (January-April). A little difference to the NR pattern, arriving peaks from PBSR are also evident in the spring of the first year. The peaking signals in the arriving patterns imply the important roles that the ocean dynamics play to transport the particles to the Galápagos Islands. The same number of particles are released from each river source every day, but not the same number arrived at the Galápagos every day. This phenomenon can only be explained by the ocean dynamics between the sources and the destination. To further investigate where the ocean dynamics take place, pathways of the Galápagos plastic are studied in section 3.2.

Compared to NR and PBSR, the NHCS arriving patterns are more averagely distributed. Within NHCS, the arriving pattern from Guayaquil seems to extend to the latter half of the second year. Although the arriving dates seems to be averagely distributed on the timeline, it does not mean that the particles from the NHCS travels randomly to the Galápagos. In

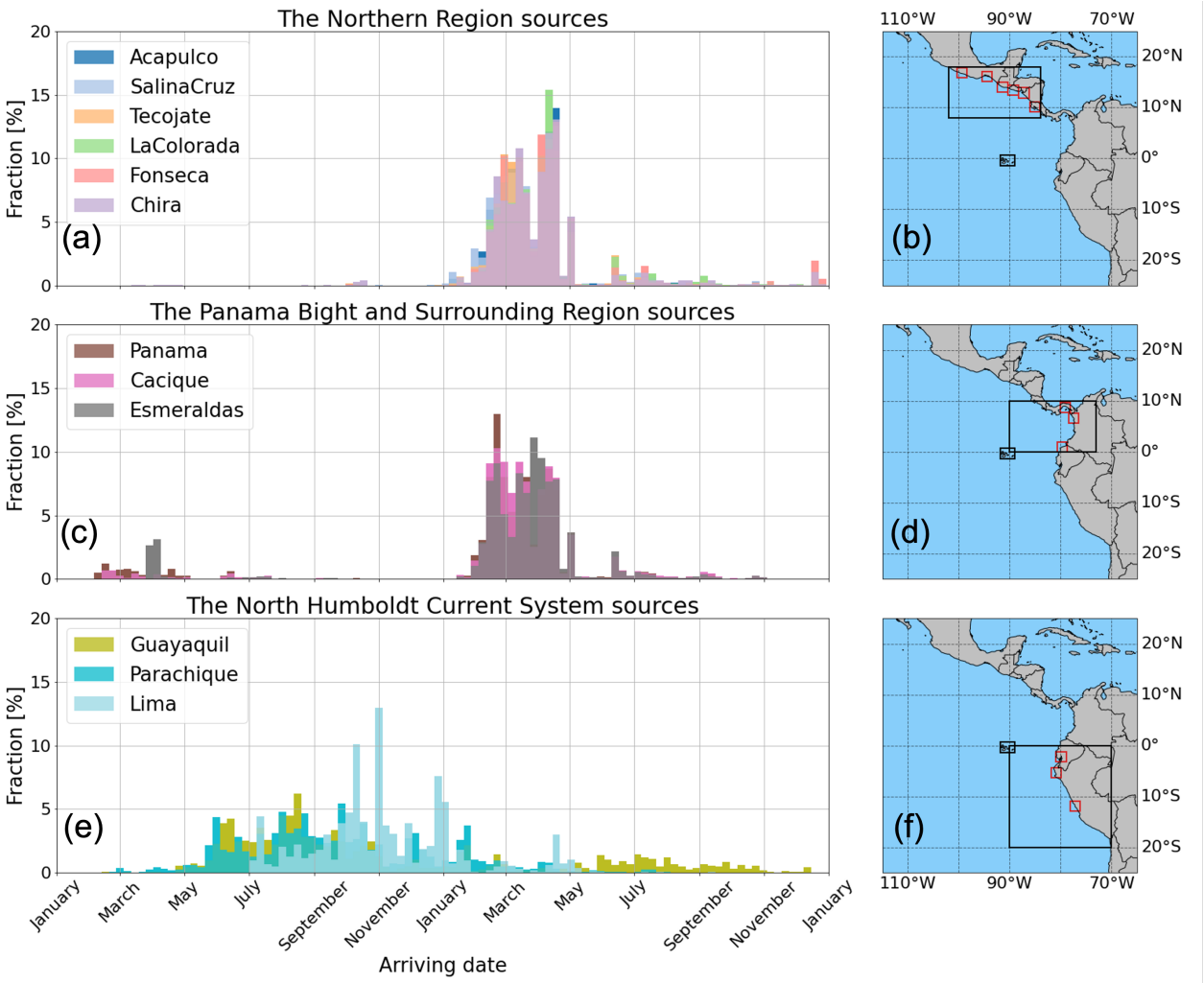


Figure 5: The three subplots show three arriving patterns from three regions. Particles are only released in the first year. The geographic locations of the three regions are shown in the black boxes in the right panel. The corresponding river sources are shown as the red boxes in the right panel.

all simulations, most particles from Parachique arrive at the Galápagos within 120 days and 180 days from Lima to the Galápagos (figure 12).

## 3.2 Process Attribution

### 3.2.1 Particle Pathways

In section 2.4.1, we introduce the occurrence density map from all 12 sources. The hotspots of the density map represent the potential particle pathways. We divide the 12 density maps into the same categories in section 3.1.2. We discover that the density maps in the same category show similarities with each other. Among the river sources for each category, the similarities in both arriving patterns and pathways indicate that the common pathways taken

by the particles can be the reason that leads to the different arriving patterns.

The two major entrances are defined in section 2.4.2 for particles into the Galápagos. Most of the particles from the NR sources arrive in the PBSR before they reach the Galápagos. Like most particles from the PBSR sources, most of the NR sourced particles take the Panama Jet Current (PJC) entrance into the Galápagos (figure 6a and 6b). The PJC entrance connects the northeast Galápagos and the PBSR. For the particles from the NHCS sources, mainly take the Humboldt Current (HC) entrance into the Galápagos (figure 6c). The HC entrance connects the east Galápagos and the Ecuador coast.

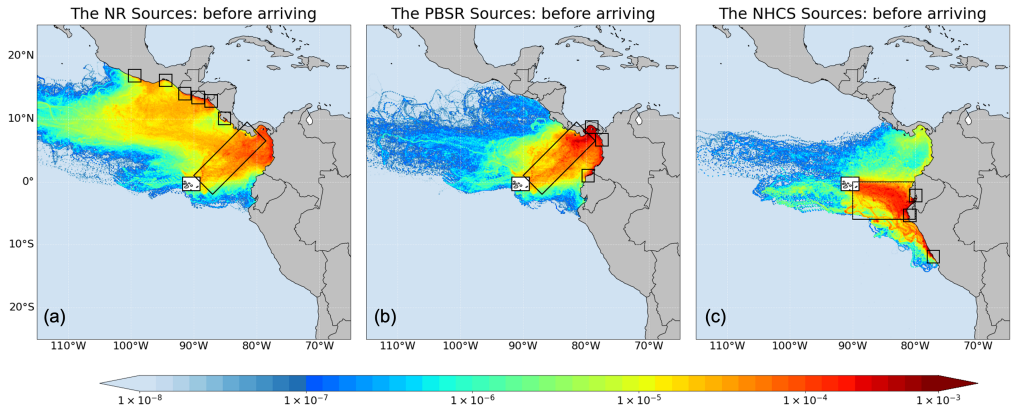


Figure 6: The occurrence density maps of sources from the three categorized regions, with (a) the Northern Region (NR) sources, (b) the Panama Bight and Surrounding Regions sources and (c) the North Humboldt Current System sources respectively. The warm colors represent for high occurrence density. The two major entrances into the Galápagos are show in the rectangular boxes, with the Panama Jet Current (PJC) in (a) and (b) and Humboldt Current (HC) in (c).

For the NR and PBSR sourced particles, nearly 40% of the particles found at the Galápagos take the PJC entrance (figure 7). For the NHCS sourced particles, more than 40% of the particles found at the Galápagos take the HC entrance (figure 7). In conclusion, the HC entrance is likely to be the major pathway for NHCS sourced particles into the Galápagos, while the PJC entrance is likely to be the major pathway for NR and PBSR sourced particles into the Galápagos

### 3.2.2 Ocean Dynamics

The flow speed and direction are sampled at daily occurrence during the 40 days before the particles arriving at the Galápagos (figure 8). High occurrence densities are observed in the corresponding entrances, which proves that the velocity field is most frequently sampled within the relevant regions. The sampled flow data shows the ocean dynamics behind the pathways and is demonstrated in the wind rose in figure 9.

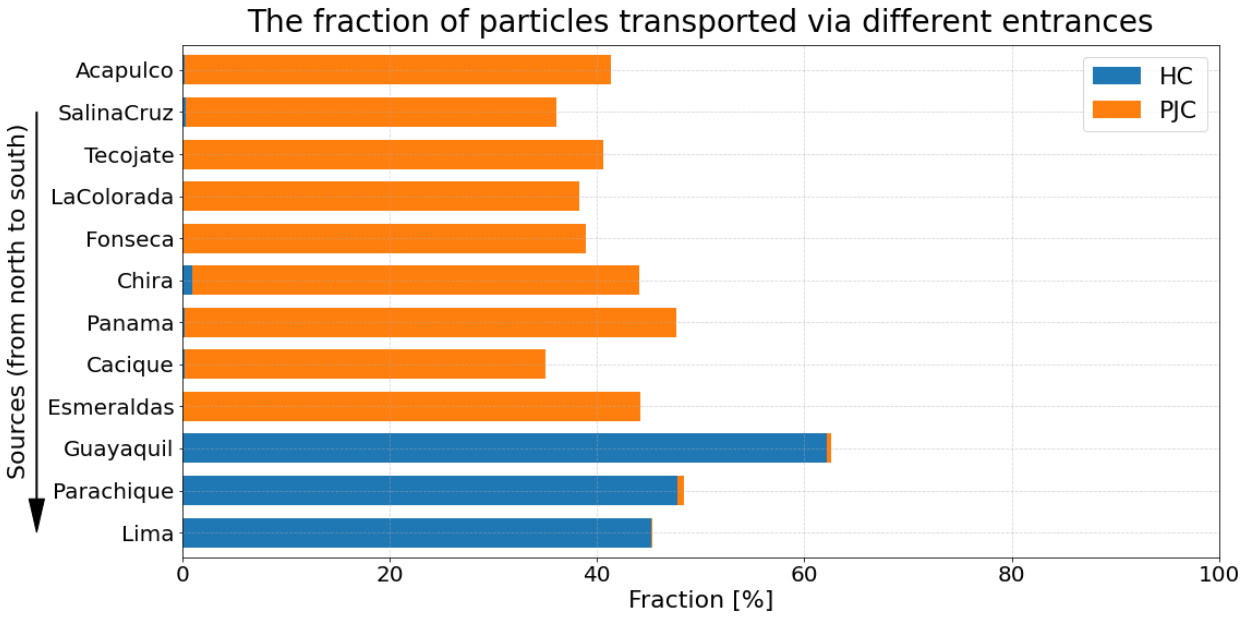


Figure 7: Fraction of the Galápagos particles transported via different entrances. The orange and blue bars show the fraction of PJC and HC entrance respectively.

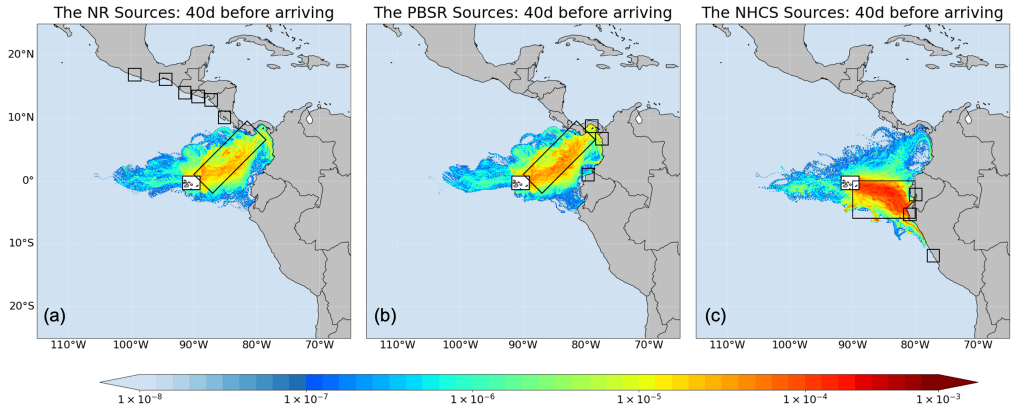


Figure 8: The occurrence density map during 40 days before the particles arrive at the Galápagos.

The flow with the speed and direction shown as green bars in the wind roses represent for more than 70% of the sampled flow occurrence. Here we define the Panama Jet Current (PJC) as a flow with a speed between 0.3 $m\,s^{-1}$ and 1.0 $m\,s^{-1}$ to the direction between 160° and 250°. The Humboldt Current (HC) is defined as a flow with speed between 0.2 $m\,s^{-1}$ and 0.6 $m\,s^{-1}$ and direction between 120° and 190°.

While the wind roses give the definitions to the potential ocean dynamics that transport the

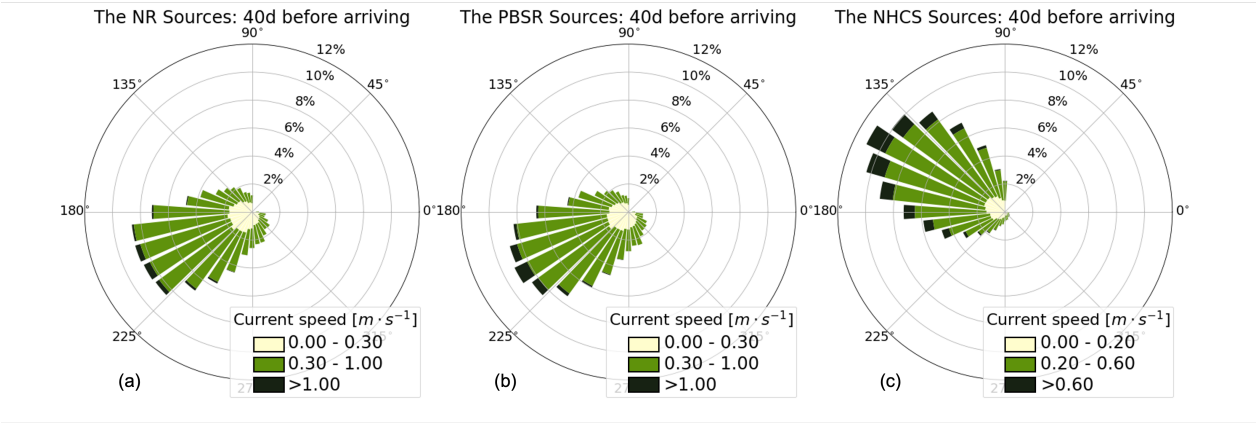


Figure 9: The sampled flow speed and direction are demonstrated in the wind rose diagrams. The sampled pathways in (a), (b) and (c) are from NR, PBSR and NHCS sources respectively. The bar direction points at the flow direction. The r axis indicates the amount of the corresponding flow.

particles, we need to further investigate the occurring time of the relevant dynamics to answer the question that if the dynamics are responsible for the arriving patterns in figure 5. The definition of the target flow defined via the wind rose is used to identify the corresponding current in the velocity field within the entrance box. The strength of the PJC is defined as the average speed of the velocity field with direction between 160° and 250°. The HC strength is averaged with direction between 120° and 190°.

The PJC strength shows a seasonal pattern, with the strength over 0.3 $m\,s^{-1}$ from January to April. Most of the Galápagos particles are transported via PJC entrance when the PJC strength is over 0.3 $m\,s^{-1}$. The particles from the NR sources are only transported through PJC entrance in the second year, while some of the particles from the PBSR sources are already transported in the first year. The possible reason for this difference is as follows. The particles released from the NR sources can not reach the inway of the entrance during January to April of the first year when the PJC is active. However, the particles from the PBSR sources can possibly reach the inway of PJC entrance in the first year when the PJC is active.

For the NR and PBSR cases, the peaks of arriving patterns are later than the transport patterns but still temporally close to the occurring time of the PJC. This is intuitively correct, since the PJC entrance is adjacent to the Galápagos region. Note that in both cases, there are arriving peaks that cannot be explained by the transport peaks during June-September (figure 10a and 10c).

The occurring time and characteristics of the PJC are in consistency with the previous research. Altimetry measurements show that the southwestward current is commonly observed higher than 0.5 m/s during January to March but remains invisible for the rest of the year (Chaigneau et al., 2006; Rodríguez-Rubio et al., 2003) And the mean surface speed in the PBSR is 0.3 m/s (Chaigneau et al., 2006).

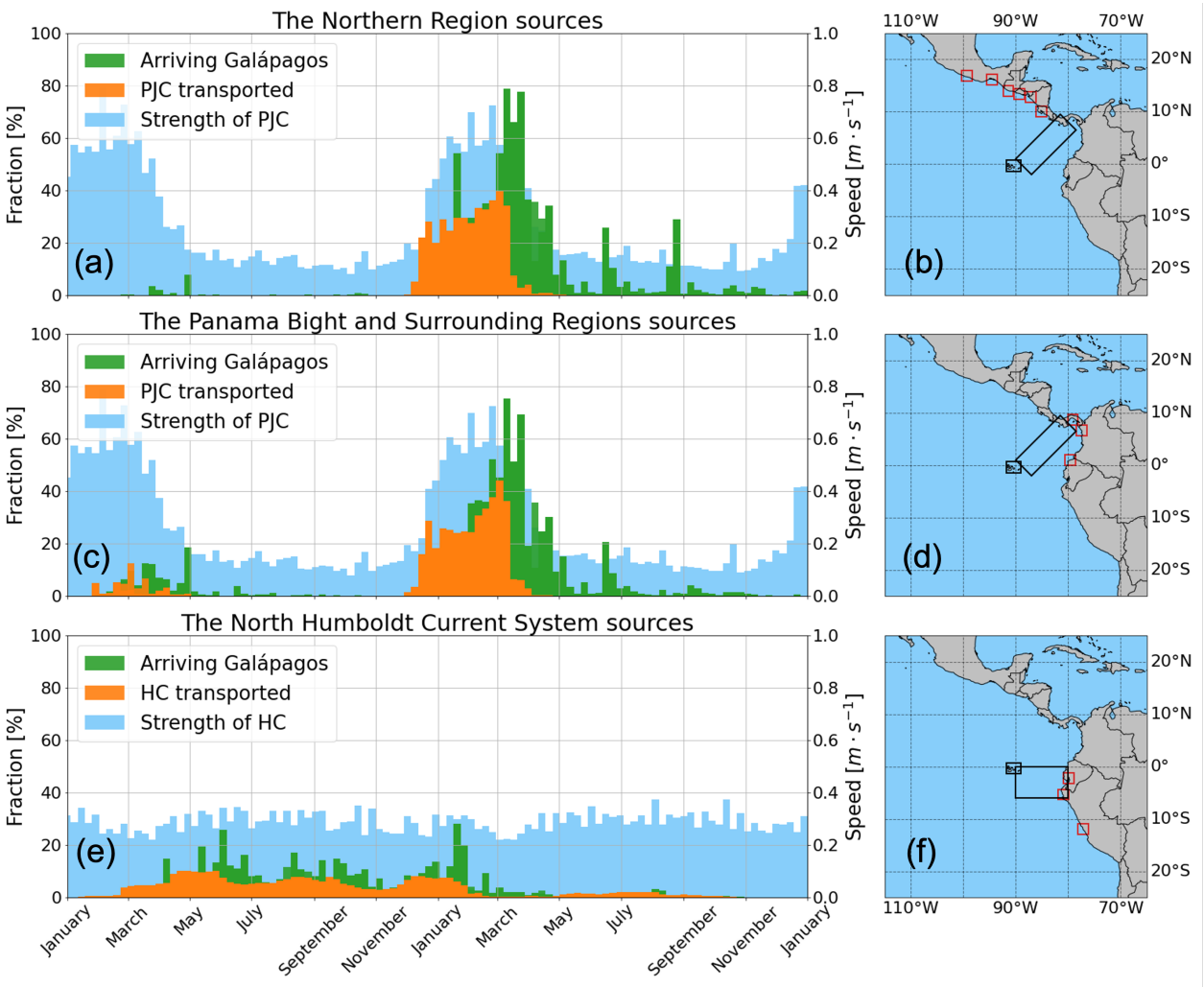


Figure 10: The left panel shows the time patterns of arriving particles (in green bars), ocean dynamics (in blue bars) and particles transported through the corresponding entrances (in orange bars). Subplots in the right panel show the geographic locations of the river sources (red boxes) and the corresponding entrances (black boxes).

There is no seasonal patterns for the HC strength, with the strength of HC over 0.2 $m\,s^{-1}$ for the whole year. Most of the particles are transported through the HC entrance during March of the first year to February of the second year. Note that particles are only released during the first year and most of the particles take less than 100 days to arrive at the Galápagos from the NHCS source. As a result, the transport pattern is expected to be most evident during the first year. For the NHCS case, the peaks of arriving patterns are also later than the transport patterns and temporally close to each other.

# 4 Discussion

In this research, we proposed three research goals to better understand the plastic arrivals at the Galápagos Islands. We introduced a Bayesian framework to estimate the attribution of the Galápagos plastic to the riverine plastic sources along the west coast of the Americas (section 2.1 and 2.3). By conducting Lagrangian simulations, we aim to discover the temporal distribution of the virtual plastic particles arriving at the Galápagos and the ocean dynamics that cause the specific arriving patterns (section 2.2 and 2.4).

12 river sources along the west coast of the Americas are considered the only plastic inputs in the study region. The attribution of the Galápagos particles to the 12 sources is conducted under a probabilistic framework based on Bayes' theorem. If a virtual plastic particle is found at the Galápagos Islands, there is a 95% probability the particle is from the Panama Bight and Surrounding Regions (PBSR), specifically 80% from Panama and 14% from Cacique. From the Bayesian framework, we know that the high attribution to the PBSR is due to both high probability of plastic inputs (table 1) and high arriving rate of the PBSR particles (left panel of figure 4). We have to release enough numbers to ensure the arriving rate is close to the real probability of the particles arriving at the Galápagos region from each source. All the analyses are repeated with only half of the particles and the results and conclusions are not affected. This indicates that we released sufficient particles.

The previous paragraph concludes Panama to be the most likely riverine source (80%) for plastic into the Galápagos, partly due to the predominant riverine plastic inputs (50%) in the region and partly owing to the second highest arriving rate (12%) of all 12 sources. However, in previous research by van Sebille et al. (2019), there are almost no particles from the coastline of Panama arriving at the Galápagos (arriving rate is 0%, from table 2). The possible reasons that lead to this difference are discussed in section 4.1.

Most of the particles released from the PBSR sources arrive at the Galápagos in boreal spring (January-April) (Figure 5c). A Low arriving rate is shown in the first year due to few particles released before the PJC event. Particles from the North Humboldt Current System (NHCS) sources arrive at the Galápagos throughout the whole year, with most arrivals during April-December (Figure 5e). The results show that there is barely any particle arriving after May in the second year, which seems contradictory to the conclusion, but the possible reason is that most of the particles arrive at the Galápagos within 120 days (figure 12) and no particles are released from the second year. Since the emission of virtual plastic particles at each river source is constant throughout the whole year, the temporal distribution of the arriving patterns can only be caused by the ocean dynamics. Specifically, the two distinct arriving patterns of the PBSR and NHCS cases are caused by two distinct ocean dynamics. The river sources in the Northern Regions (NR) are geographically far away from the PBSR sources, but arriving pattern of the NR case is identical to the PBSR case, which possibly indicates the same dynamic behind the phenomenon.

The particle pathways from the NR and PBSR sources indeed share the same entrance that transports particles to the Galápagos from the northeast direction. The entrance is defined as the Panama Jet Current (PJC) entrance and is responsible for transporting around 40%

of the particles that eventually arrive at the Galápagos. As we expected, the PJC transport has a similar seasonal pattern to the arriving patterns in both NR and PBSR cases (figure 10a and 10c). The transport is driven by the Panama Jet Current, defined as a flow with a speed over 0.3 $m\,s^{-1}$, a direction between 160° and 250°. The Panama Jet Current occurs during December-March. So we conclude that the PJC is the direct cause for the NR and PBSR sourced particles arriving at the Galápagos in boreal winter.

The particles from the NHCS enter the Galápagos from the Humboldt Current (HC) entrance, connecting east Galápagos to the offshore region of northern Peru. More than 40% of the particles that arrive at the Galápagos are transported through the HC entrance. The HC transport takes place throughout the year which is similar to the arriving patterns in the NHCS case (figure 10e). The HC transport is driven by the Humboldt Current, defined as a flow with a speed between 0.2 $m\,s^{-1}$ and 0.6 $m\,s^{-1}$ and a direction between 120° and 190°. The Humboldt Current does not have a seasonal variation in speed and direction and is the direct cause for the particle arrivals at the Galápagos from NHCS sources.

Multiple ocean dynamics take place along the particle pathways, but only two ocean currents are resolved in this research (section 3.2.2). The compromise is made mainly due to the limited time of the project. The possible dynamics that have not been resolved are discussed in section 4.2.

In addition, the PJC is responsible for only 40% of the seasonal arrivals, which means there are probably other dynamics responsible. (Chaigneau et al., 2006) points out that the eddy activity is also seasonal active, double in winter than during summer. The PJC behavior defined in section 2.4.3 can hardly identify any eddy behaviors of particles, which results in failure of identifying ocean eddies that transport the particles.

## 4.1 Comparison with Results by van Sebille

Lagrangian simulations are done by van Sebille et al. (2019) to study the pathways of particles released from the west coast of the Americas. Two sets of simulations are conducted in their research, one with only the currents and the other with both currents and waves. The arriving rate is calculated at each releasing location (figure 5 from van Sebille et al. (2019)). However, the 12 river sources are not all included by van Sebille et al. (2019). As a result, the arriving rate at the river that is not simulated is interpolated between the adjacent data. In both research, the arriving rate from Parachique is the highest of all 12 sources. However, compared with the current-only results by van Sebille et al. (2019), there are a few differences in the results from this research (column 2 and 3 in table 2). While in this research, the second highest arriving rate is from Panama (12.4%), in the research from van Sebille et al. (2019), the arriving rate from Panama is 0.0%. Apart from the big difference in Panama and Cacique, arriving rates from the rest 11 river sources by van Sebille et al. (2019) slightly deviate from the results in this research. The small difference in arriving rate is due to the different simulation periods and ocean general circulation model used in the two research. But the big deviance in Panama is explained by the releasing methods. van Sebille et al. (2019) released one particle each 0.5° between $38°S$ and $31°N$ every 5 days along the

Table 2: Arriving rate of the particles released from the 12 river sources. Column 2 shows the result in this research. Column 3 and 4 show the result by van Sebille et al. (2019). The results in column 3 are from simulations considering only ocean currents, while the results in column 4 are from simulations including both ocean currents and waves

| River source | This research | Currents only | Currents & Waves |
|---|---|---|---|
| Acapulco | 1.4% | 2.0% | 0.0% |
| Salina Cruz | 1.7% | 2.1% | 0.0% |
| Tecojate | 1.3% | 2.2% | 0.0% |
| La Colorada | 1.0% | 2.5% | 0.0% |
| Fonseca | 0.7% | 3.0% | 0.0% |
| Chira | 1.4% | 2.8% | 0.0% |
| Panama | 12.4% | 0.0% | 0.0% |
| Cacique | 11.4% | 6.5% | 0.0% |
| Esmeraldas | 3.7% | 4.0% | 0.0% |
| Guayaquil | 2.6% | 3.9% | 1.9% |
| Parachique | 23.4% | 18.0% | 17.0% |
| Lima | 1.0% | 2.8% | 0.0% |

coastline. The releasing method works well when there are no U-curves on coastlines. A big part of the U-curve coastline is skipped when adopting this releasing method and that is what happened in Panama bay, where Panama locate. As a result, the location of the Panama source in this research is not selected as a releasing source by van Sebille et al. (2019), which might have lead to the 0.0% arriving rate in their research.

## 4.2 Other Dynamics

Multiple ocean dynamics take place along the particle pathways, but only two ocean currents are resolved in this research (section 3.2.2). The compromise is made mainly due to the limited time of the project. The possible dynamics that have not been resolved are discussed in the following section.

### 4.2.1 Stokes Drift and Windage Transport

Wind stress can not only drive currents but also the waves. Stokes drift is the net drift velocity in the direction of wave propagation experienced by a particle floating at the free surface of a water wave (van den Bremer and Breivik, 2018). Stokes drift is incorporated by van Sebille et al. (2019) in the simulations (currents+waves) of particle pathways from the west coast of the Americas to the Galápagos and the results are compared with the only-currents scenario. The arriving rates of the currents+waves scenario are zero from most of the sources, except for Guayaquil (1.9%) and Parachique (17.0%). As Stokes drift is incorporated, the particles are less likely to reach the Galápagos in general, partly because the waves constantly push particles eastward onto the shore so that they had less chance of reaching the open ocean (van

Sebille et al., 2019). However, the arriving rate from Parachique seems to be less affected. The comparison between two scenarios by van Sebille et al. (2019) indicates that attribution of the river sources in this research might be affected as well.

The wind stress can also have a direct effect on the floating debris with a freeboard, which is termed windage transport. Apart from the strength of wind stress itself, the density, shape and size of plastic have a combined effect on the strength of windage (Zambianchi, 2014; Ryan, 2015; Chubarenko et al., 2016; Pereiro et al., 2018), and hence their dispersion (Zambianchi, 2014), which ultimately affects both residence time and beaching characteristics of floating items (Yoon et al., 2010). Maximenko et al. (2018) validate the model simulations of floating debris generated by the 2011 tsunami in Japan with observation data. The results show that the different strength of windage leads to different particle pathways.

The windage and Stokes drift are all missing in this research, but these two processes are recommended to be added in future research on the simulations of particle pathways and source attribution. In order to model the processes more accurately, more field observations are needed to validate the model results.

### 4.2.2 Biofouling and 3D Structure of Flow Field

In the real world, various plastic properties can affect the interactions between plastic and the environment. Density and size are the most concerned parameters. In this research, we assume the particles are positively buoyant and relatively large plastic (plastic density smaller than seawater density). When the size of the plastic is smaller to an extent, biofouling takes place and causes a vertical movement in the plastic behavior (Kooi et al., 2017). Biofouling is a phenomenon where biofilm grows on plastic and makes the particle negatively buoyant. In the biofouling model proposed by Kooi et al. (2017), a low-density polyethylene plastic particle (radius: 10mm) takes around 30 days to start sinking. In this research, the particles from all the river sources spend more than 30 days arriving at the Galápagos. If biofouling was considered, the vertical particle movements and vertical advection of the ocean flow would affect the particle trajectories.

The South Equatorial Current (SEC) is the dominant westward surface flow in the Eastern Tropical Pacific. However, the region is considered with a more complex 3D feature in the current circulation. Kessler (2006) concluded that the Equatorial Undercurrent (EUC) is much larger than Humboldt Current to feed the SEC. The EUC surfaces during boreal spring change the sub-surface flow in the study region eastward during the average April and May (Reverdin et al., 1994; Kessler et al., 1998). So if part of the particle trajectories reaches a deeper level along the pathways and encounters the EUC, fewer particles might have been found at the Galápagos, thus leading to a decrease in the arriving.

## 4.3 Future Research

The methodology of combining Lagrangian simulation and Bayesian framework is used in this research to attribute the riverine plastic sources. In future research, we can extend the scope of the methods to other plastic sources, such as direct inputs along the coastlines,

shipping, fisheries and the Great Pacific Garbage Patch. It has been approved applicable to incorporate biofouling (Lobelle et al., 2021) and Stokes drift (van Sebille et al., 2019) in Lagrangian simulations. For analysis methods, it is necessary to come up with methods to identify and quantify the eddy behaviors of particles in numerical simulations.

# 5 Conclusion

The aim of this research is to obtain more information on the plastic arrivals at the Galápagos Islands. Specifically, the goal is to attribute the plastic found at the Galápagos to the major riverine plastic sources along the west coast of the Americas, discover the temporal distribution of the plastic arriving at the Galápagos region and identify the major ocean dynamics that is responsible for the plastic arriving at certain time. Lagrangian simulations are conducted to discover arriving time and pathways of the particles from the river sources to the Galápagos (section 2.2 and 2.4). A Bayesian framework is used to make attribution to the river sources (section 2.1 and 2.3).

The river source at Panama is a predominant riverine plastic source in the study region ($25°S$-$25°N$), contributing 50% of the inputs to the ocean. The Panama Bight and Surrounding Regions (PBSR) sources are most likely to be the origin for the plastic found at the Galápagos (with a probability of 95%, including Panama 80% and Cacique 14%). The particles from the PBSR sources only arrive at the Galápagos region in boreal spring (January-April) and the pathways all converge within the PBSR. Eventually, the particles take an entrance that cross the PBSR from northeast corner to southwest corner into the Galápagos. This entrance is also the major pathway for the particles sourced from the Norther Region (NR) into the Galápagos. These results makes the PBSR a very important region to study the seasonal arrivals of the plastic at the Galápagos. A current with speed over $0.3\ m\,s^{-1}$, direction between 160° and 250° is discovered and defined as the Panama Jet Current (PJC). The location of the PJC is found between $9°N$-0° and $90°W$-$80°W$ tilted in the 'northeast-southwest' direction. The ocurring time of the PJC is during January-April. The previous researchers have identify this seasonal jet current to some extent, but never propose an explicit definition on it.

In future research, it is recommended to add biofouling and Stokes drift into the numerical model in order to increase the authenticity of the model. New methods to identify and quantify the eddy behaviors of the virtual particles are needed. The future availability of observation data would be of great help to validate the model results constructed in this research.

# 6 Appendices

## 6.1 Arriving patterns

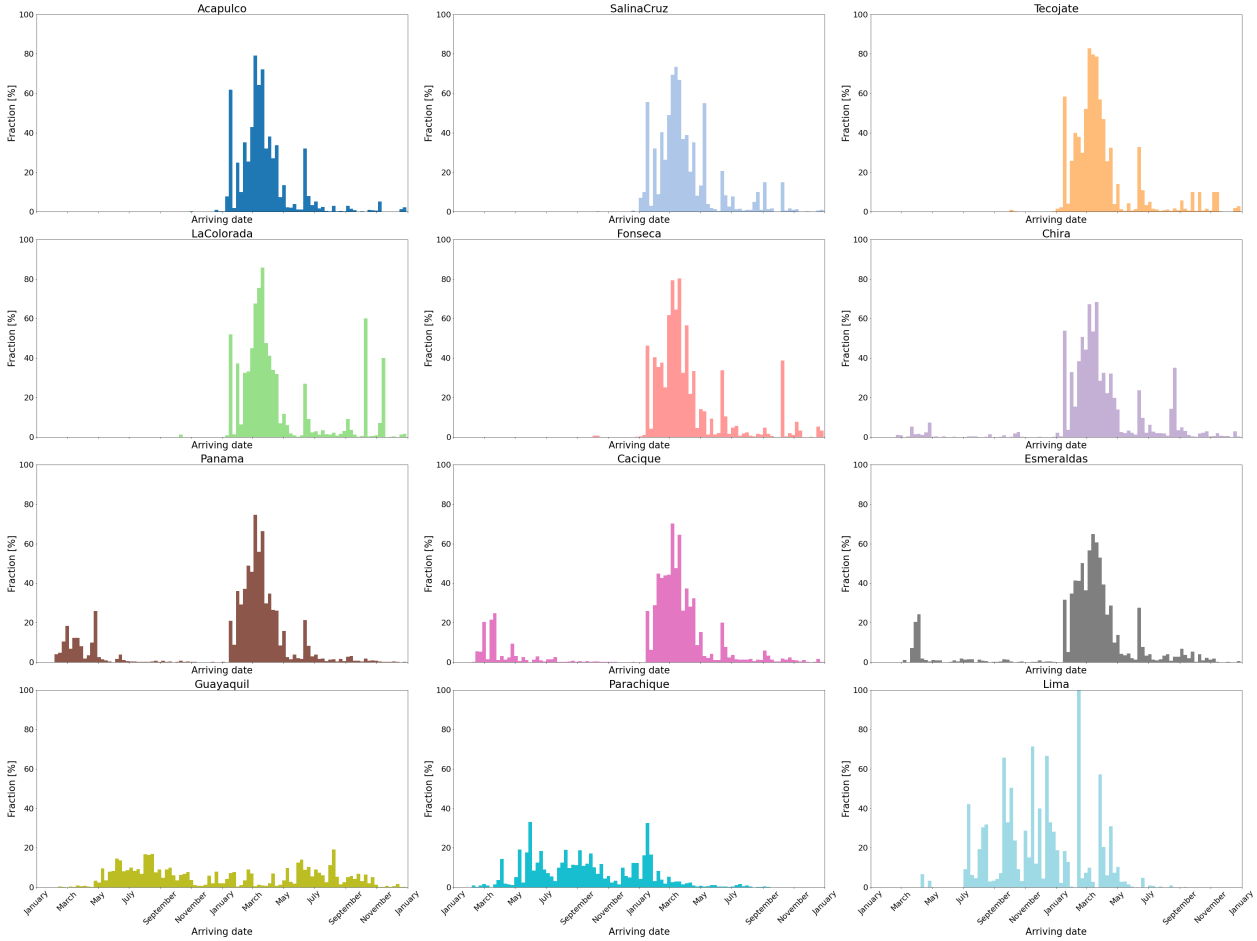


Figure 11: The arriving patterns for all 12 sources, averaged over 14 simulations.

## 6.2 Age distribution

The age of a particle is defined as the travel time from it is released till it arrives at the Galápagos

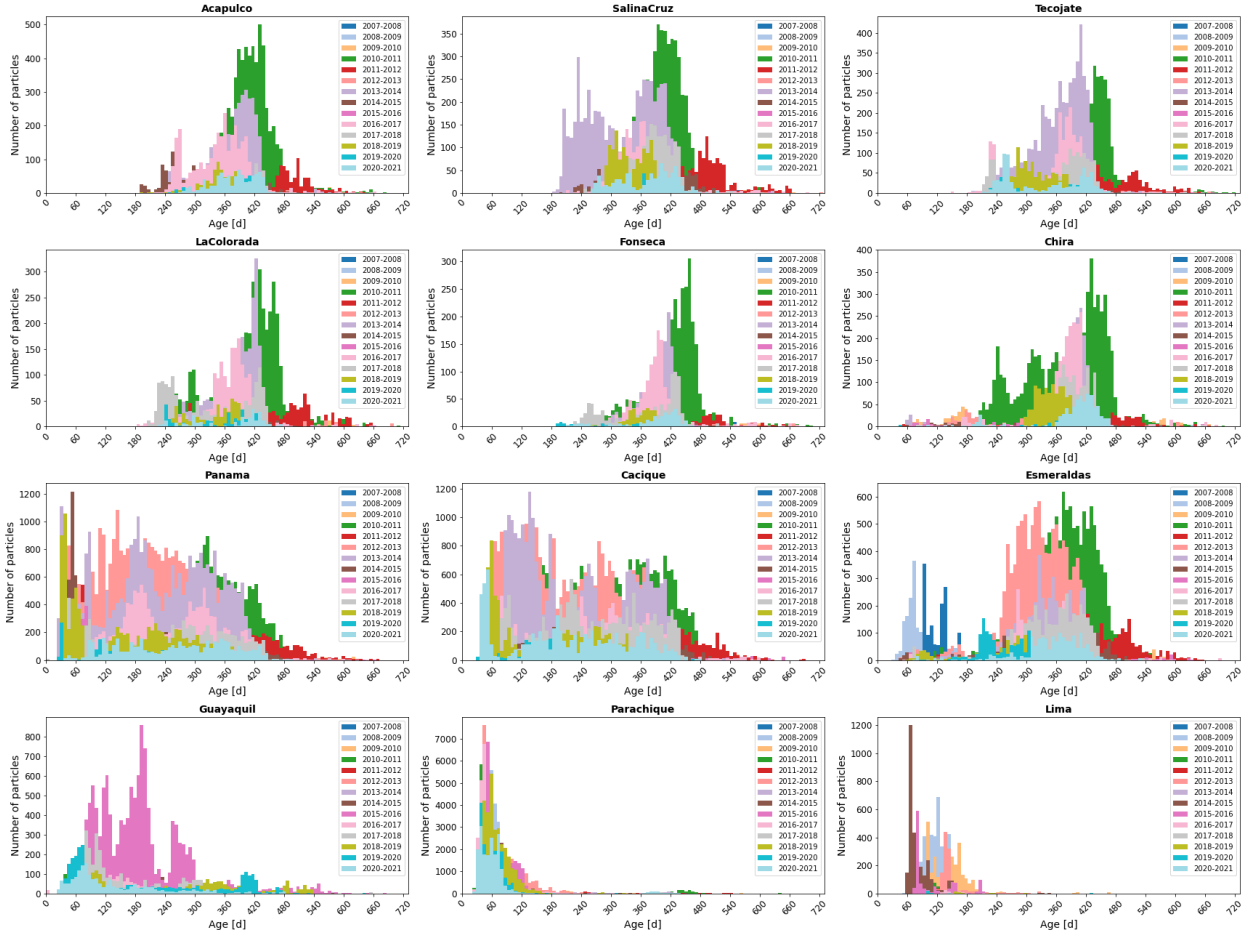


Figure 12: The age distribution patterns for all 12 sources, averaged over 14 simulations

# References

Barnes, D. K., Walters, A., and Goncalves, L. (2010). Macroplastics at sea around antarctica. *Mar Environ Res*, 70(2):250–2.

Buhl-Mortensen, L. and Buhl-Mortensen, P. (2017). Marine litter in the nordic seas: Distribution composition and abundance. *Mar Pollut Bull*, 125(1-2):260–270.

Carlin, B. P., . L. T. A. (2008). *Bayesian methods for data analysis*. CRC Press.

Carretero, O., Gago, J., Filgueiras, A. V., and Vinas, L. (2022). The seasonal cycle of micro and meso-plastics in surface waters in a coastal environment (ria de vigo, nw spain). *Sci Total Environ*, 803:150021.

Chaigneau, A., Abarca del Rio, R., and Colas, F. (2006). Lagrangian study of the panama bight and surrounding regions. *Journal of Geophysical Research*, 111(C9).

Cheung, P. K., Fok, L., Hung, P. L., and Cheung, L. T. O. (2018). Spatio-temporal comparison of neustonic microplastic density in hong kong waters under the influence of the pearl river estuary. *Sci Total Environ*, 628-629:731–739.

Chubarenko, I., Bagaev, A., Zobkov, M., and Esiukova, E. (2016). On some physical and dynamical properties of microplastic particles in marine environment. *Mar Pollut Bull*, 108(1-2):105–12.

Cozar, A., Marti, E., Duarte, C. M., Garcia-de Lomas, J., van Sebille, E., Ballatore, T. J., Eguiluz, V. M., Gonzalez-Gordillo, J. I., Pedrotti, M. L., Echevarria, F., Trouble, R., and Irigoien, X. (2017). The arctic ocean as a dead end for floating plastics in the north atlantic branch of the thermohaline circulation. *Sci Adv*, 3(4):e1600582.

Delandmeter, P. and van Sebille, E. (2019). The parcels v2.0 lagrangian framework: new field interpolation schemes. *Geoscientific Model Development*, 12(8):3571–3584.

Derraik, J. G. B. (2002). The pollution of the marine environment by plastic debris: a review. *Marine Pollution Bulletin*, 44(9):842–852.

Doong, D. J., Chuang, H. C., Shieh, C. L., and Hu, J. H. (2011). Quantity, distribution, and impacts of coastal driftwood triggered by a typhoon. *Mar Pollut Bull*, 62(7):1446–54.

Dris, R., Imhof, H., Sanchez, W., Gasperi, J., Galgani, F., Tassin, B., and Laforsch, C. (2015). Beyond the ocean: contamination of freshwater ecosystems with (micro-)plastic particles. *Environmental Chemistry*, 12(5).

Faris, Jeannie;Hart, K. (1994). *Seas of debris: a summary of the third international conference on marine debris*. CRC Press.

Geyer, R., Jambeck, J. R., and Law, K. L. (2017). Production, use, and fate of all plastics ever made. *Sci Adv*, 3(7):e1700782.

Ghiggi, G., Humphrey, V., Seneviratne, S. I., and Gudmundsson, L. (2019). Grun: an observation-based global gridded runoff dataset from 1902 to 2014. *Earth System Science Data*, 11(4):1655–1674.

Grados, C., Chaigneau, A., Echevin, V., and Dominguez, N. (2018). Upper ocean hydrology of the northern humboldt current system at seasonal, interannual and interdecadal scales. *Progress in Oceanography*, 165:123–144.

Jambeck, J. R., Geyer, R., Wilcox, C., Siegler, T. R., Perryman, M., Andrady, A., Narayan, R., and Law, K. L. (2015). Marine pollution. plastic waste inputs from land into the ocean. *Science*, 347(6223):768–71.

Jiang, Y., Zhao, Y., Wang, X., Yang, F., Chen, M., and Wang, J. (2020). Characterization of microplastics in the surface seawater of the south yellow sea as affected by season. *Sci Total Environ*, 724:138375.

Jones, J. S., Porter, A., Munoz-Perez, J. P., Alarcon-Ruales, D., Galloway, T. S., Godley, B. J., Santillo, D., Vagg, J., and Lewis, C. (2021). Plastic contamination of a galapagos island (ecuador) and the relative risks to native marine species. *Sci Total Environ*, 789:147704.

Kaandorp, M. L. A., Ypma, S. L., Boonstra, M., Dijkstra, H. A., and van Sebille, E. (2022). Using machine learning and beach cleanup data to explain litter quantities along the dutch north sea coast. *Ocean Science*, 18(1):269–293.

Kessler, W. S. (2002). Mean three-dimensional circulation in the northeast tropical pacific*. *Journal of Physical Oceanography*, 32(9):2457–2471.

Kessler, W. S. (2006). The circulation of the eastern tropical pacific: A review. *Progress in Oceanography*, 69(2-4):181–217.

Kessler, W. S., Rothstein, L. M., and Chen, D. (1998). The annual cycle of sst in the eastern tropical pacific, diagnosed in an ocean gcm*. *Journal of Climate*, 11(5):777–799.

Kooi, M., Nes, E. H. v., Scheffer, M., and Koelmans, A. A. (2017). Ups and downs in the ocean: Effects of biofouling on vertical transport of microplastics. *Environmental Science Technology*, 51(14):7963–7971.

Lavers, J. L. and Bond, A. L. (2017). Exceptional and rapid accumulation of anthropogenic debris on one of the world's most remote and pristine islands. *Proceedings of the National Academy of Sciences*, 114(23):6052–6055.

Lebreton, L. and Andrady, A. (2019). Future scenarios of global plastic waste generation and disposal. *Palgrave Communications*, 5(1).

Lebreton, L., Egger, M., and Slat, B. (2019). A global mass budget for positively buoyant macroplastic debris in the ocean. *Sci Rep*, 9(1):12922.

Lebreton, L. C., Greer, S. D., and Borrero, J. C. (2012). Numerical modelling of floating debris in the world's oceans. *Mar Pollut Bull*, 64(3):653–61.

Lima, A. R., Costa, M. F., and Barletta, M. (2014). Distribution patterns of microplastics within the plankton of a tropical estuary. *Environ Res*, 132:146–55.

Lithner, D., Larsson, A., and Dave, G. (2011). Environmental and health hazard ranking and assessment of plastic polymers based on chemical composition. *Sci Total Environ*, 409(18):3309–24.

Liu, T., Zhao, Y., Zhu, M., Liang, J., Zheng, S., and Sun, X. (2020). Seasonal variation of micro- and meso-plastics in the seawater of jiaozhou bay, the yellow sea. *Mar Pollut Bull*, 152:110922.

Lobelle, D., Kooi, M., Koelmans, A. A., Laufkotter, C., Jongedijk, C. E., Kehl, C., and van Sebille, E. (2021). Global modeled sinking characteristics of biofouled microplastic. *J Geophys Res Oceans*, 126(4):e2020JC017098.

Maximenko, N., Hafner, J., Kamachi, M., and MacFadyen, A. (2018). Numerical simulations of debris drift from the great japan tsunami of 2011 and their verification with observational reports. *Mar Pollut Bull*, 132:5–25.

Meijer, L. J. J., van Emmerik, T., van der Ent, R., Schmidt, C., and Lebreton, L. (2021). More than 1000 rivers account for 80emissions into the ocean. *Sci Adv*, 7(18).

Mestanza, C., Botero, C. M., Anfuso, G., Chica-Ruiz, J. A., Pranzini, E., and Mooser, A. (2019). Beach litter in ecuador and the galapagos islands: A baseline to enhance environmental conservation and sustainable beach tourism. *Mar Pollut Bull*, 140:573–578.

Onink, V., Jongedijk, C. E., Hoffman, M. J., van Sebille, E., and Laufkötter, C. (2021). Global simulations of marine plastic transport show plastic trapping in coastal zones. *Environmental Research Letters*, 16(6).

Pereiro, D., Souto, C., and Gago, J. (2018). Calibration of a marine floating litter transport model. *Journal of Operational Oceanography*, 11(2):125–133.

Pierard, C. M., Bassotto, D., Meirer, F., and van Sebille, E. (2022). Attribution of plastic sources using bayesian inference: Application to river-sourced floating plastic in the south atlantic ocean. *Frontiers in Marine Science*, 9.

Reverdin, G., Frankignoul, C., Kestenare, E., and McPhaden, M. J. (1994). Seasonal variability in the surface currents of the equatorial pacific. *Journal of Geophysical Research*, 99(C10).

Rodríguez-Rubio, E., Schneider, W., and Abarca del Río, R. (2003). On the seasonal circulation within the panama bight derived from satellite observations of wind, altimetry and sea surface temperature. *Geophysical Research Letters*, 30(7).

Ryan, P. G. (2015). Does size and buoyancy affect the long-distance transport of floating debris? *Environmental Research Letters*, 10(8).

Schmidt, C., Krauth, T., and Wagner, S. (2017). Export of plastic debris by rivers into the sea. *Environ Sci Technol*, 51(21):12246–12253.

Tsang, Y. Y., Mak, C. W., Liebich, C., Lam, S. W., Sze, E. T. P., and Chan, K. M. (2020). Spatial and temporal variations of coastal microplastic pollution in hong kong. *Mar Pollut Bull*, 161(Pt B):111765.

van den Bremer, T. S. and Breivik, O. (2018). Stokes drift. *Philos Trans A Math Phys Eng Sci*, 376(2111).

van Sebille, E., Delandmeter, P., Schofield, J., Hardesty, B. D., Jones, J., and Donnelly, A. (2019). Basin-scale sources and pathways of microplastic that ends up in the galápagos archipelago. *Ocean Science*, 15(5):1341–1349.

Wagner, M., Scherer, C., Alvarez-Muñoz, D., Brennholt, N., Bourrain, X., Buchinger, S., Fries, E., Grosbois, C., Klasmeier, J., Marti, T., Rodriguez-Mozaz, S., Urbatzka, R., Vethaak, A. D., Winther-Nielsen, M., and Reifferscheid, G. (2014). Microplastics in freshwater ecosystems: what we know and what we need to know. *Environ Sci Eur*, 26(1):12.

Waller, C. L., Griffiths, H. J., Waluda, C. M., Thorpe, S. E., Loaiza, I., Moreno, B., Pacherres, C. O., and Hughes, K. A. (2017). Microplastics in the antarctic marine system: An emerging area of research. *Sci Total Environ*, 598:220–227.

Woodall, L. C., Sanchez-Vidal, A., Canals, M., Paterson, G. L., Coppock, R., Sleight, V., Calafat, A., Rogers, A. D., Narayanaswamy, B. E., and Thompson, R. C. (2014). The deep sea is a major sink for microplastic debris. *R Soc Open Sci*, 1(4):140317.

Wooster, W. (1959). Oceanographic observations in the panama bight, "askoy" expedition, 1941. *Bulletin of the American Museum of Natural History*, 118(3):117–150.

Yoon, J. H., Kawano, S., and Igawa, S. (2010). Modeling of marine litter drift and beaching in the japan sea. *Mar Pollut Bull*, 60(3):448–63.

Zambianchi, E., I. I. S. G. A. S. (2014). Marine litter in the mediterranean sea: an oceanographic perspective.